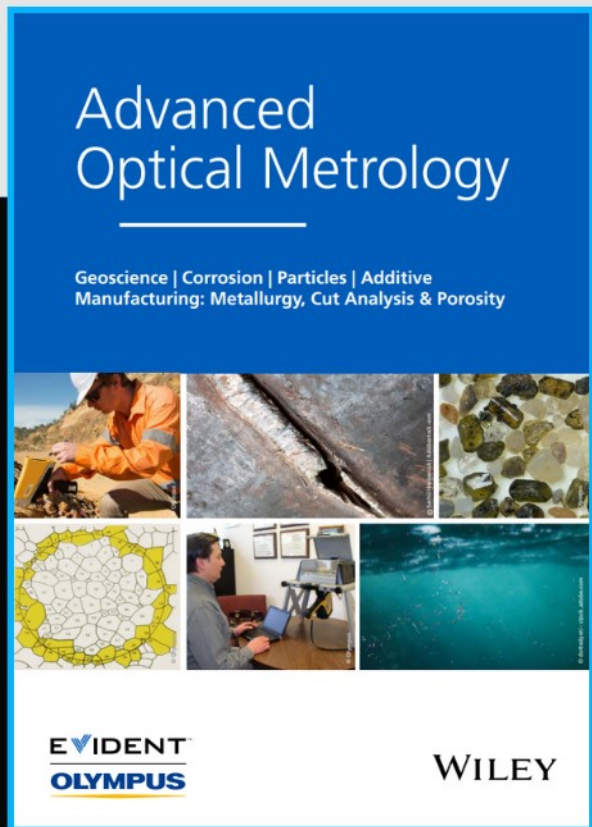




# 2<sup>nd</sup> Advanced Optical Metrology Compendium



**The latest eBook from  
Advanced Optical Metrology.  
Download for free.**

This compendium includes a collection of optical metrology papers, a repository of teaching materials, and instructions on how to publish scientific achievements.

With the aim of improving communication between fundamental research and industrial applications in the field of optical metrology we have collected and organized existing information and made it more accessible and useful for researchers and practitioners.

**EVIDENT<sup>™</sup>**  
**OLYMPUS**

**WILEY**

# Achieving Superplastic Elongations in an AZ80 Magnesium Alloy Processed by High-Pressure Torsion

Saad A. Alsubaie, Piotr Bazarnik, Yi Huang,\* Malgorzata Lewandowska, and Terence G. Langdon

High-pressure torsion (HPT) is a technique used successfully to refine the grains of an alloy to the submicrometer and nanometer scale. Grain refinement can improve the mechanical properties of magnesium alloys as well as enhancing its ductility and providing a potential for exhibiting superplastic behavior at elevated temperature. Research is conducted to process the AZ80 magnesium alloy by HPT at room temperature for different numbers of turns with the microstructures before and after HPT investigated using scanning electron microscopy (SEM), transmission electron microscopy (TEM), and Vickers microhardness (Hv) tests. Subsequently, tensile specimens are cut from the processed disks and pulled in tension to failure at temperatures of 473, 523, and 573 K and at strain rates in the range from  $1.4 \times 10^{-4}$  to  $1.4 \times 10^{-1} \text{ s}^{-1}$ . The introduction of superplasticity in the HPT-processed AZ80 is demonstrated for the first time with a maximum elongation of 645% at a testing temperature of 573 K. There is also evidence for low-temperature superplasticity with an elongation of 423% at 473 K. The dominant mechanism for superplastic flow is grain boundary sliding with a strain rate sensitivity of  $m = 0.5$  and an activation energy of  $Q = 73 \text{ kJ mol}^{-1}$ .

## 1. Introduction


Magnesium alloys have low density and lightweight being about 35% and 78% lighter than aluminum and steel, respectively. Therefore, they are attractive materials for use as structural components where weight reduction is important as in reducing fuel consumption and CO<sub>2</sub> emissions in automotive and aerospace applications.<sup>[1,2]</sup> Nevertheless, the practical applications of magnesium alloys are limited due to their hexagonal close-packed crystal structure which produces a generally poor formability at low temperatures. There are only two active independent slip

systems on the basal plane and this means that magnesium does not fulfill the requirement of five independent slip systems that are necessary for uniform deformation.<sup>[3]</sup> Twinning also operates at low temperatures and slip on nonbasal planes, such as the prismatic and pyramidal systems, may be activated by processing the alloys at elevated temperatures.<sup>[4]</sup>

Thermomechanical processing may be used to improve the mechanical properties of Mg alloys but this is usually conducted at high temperatures to avoid the limitation of the number of active slip systems. Recently, much attention has centered on the processing of metals through the application of severe plastic deformation (SPD) in procedures where high strains are imposed but without incurring any significant changes in the overall dimensions of the samples.<sup>[5–7]</sup> These procedures produce significant grain refinement, typically to

the submicrometer or nanometer scale, and invariably they lead to considerable improvements in the physical and mechanical properties of the materials. Several SPD techniques are now available but the most attractive are equal-channel angular pressing (ECAP)<sup>[8]</sup> and high-pressure torsion (HPT).<sup>[9]</sup> However, the ECAP of magnesium alloys is invariably conducted at an elevated temperature and considerable care must be exercised to avoid the development of cracks and segmentation in the test samples.<sup>[10,11]</sup> By contrast, processing by HPT is attractive because the imposition of a large hydrostatic pressure during the processing operation is effective in preventing the development of any

S. A. Alsubaie  
Department of Manufacturing Engineering  
College of Technological Studies  
P.A.A.E.T  
P.O. Box 42325, Shuwaikh 70654, Kuwait

 The ORCID identification number(s) for the author(s) of this article can be found under <https://doi.org/10.1002/adem.202200620>.

© 2022 The Authors. Advanced Engineering Materials published by Wiley-VCH GmbH. This is an open access article under the terms of the Creative Commons Attribution-NonCommercial-NoDerivs License, which permits use and distribution in any medium, provided the original work is properly cited, the use is non-commercial and no modifications or adaptations are made.

DOI: 10.1002/adem.202200620

P. Bazarnik, M. Lewandowska  
Faculty of Materials and Engineering  
Warsaw University of Technology  
Woloska 141, 02-507 Warsaw, Poland

Y. Huang  
Department of Design and Engineering  
Faculty of Science and Technology  
Bournemouth University  
Poole, Dorset BH12 5BB, UK  
E-mail: yhuang2@bournemouth.ac.uk

Y. Huang, T. G. Langdon  
Materials Research Group  
Department of Mechanical Engineering  
University of Southampton  
Southampton SO17 1BJ, UK

cracking or segmentation.<sup>[12]</sup> The principles and practices associated with the processing of Mg alloys by HPT were reviewed recently.<sup>[13]</sup>

The occurrence of superplastic flow in samples tested in tension refers specifically to the ability to develop elongations of at least 400% when the associated strain rate sensitivity,  $m$ , is close to  $\approx 0.5$  where  $m = \partial \ln \sigma / \partial \ln \dot{\epsilon}$ , where  $\sigma$  is the flow stress and  $\dot{\epsilon}$  is the imposed strain rate.<sup>[14]</sup> In practice, the development of superplasticity is important because it provides the potential for using these materials in superplastic forming operations.<sup>[15]</sup>

In practice, there are now several reports documenting the development of high tensile ductilities in a range of materials processed using SPD techniques with a record-breaking superplastic elongation of 3050% recorded in an ZK60 magnesium alloy after processing by ECAP and then testing in tension at 473 K under a strain rate of  $1.0 \times 10^{-4} \text{ s}^{-1}$ .<sup>[16]</sup> There are several reports describing the development of superplasticity in different alloys after processing by HPT<sup>[17–19]</sup> but the first report of superplasticity in a magnesium alloy processed by HPT was by Kulyasova et al. in 2006.<sup>[20]</sup> Subsequently, there were several additional reports of superplastic flow in Mg alloys processed by HPT and these data are summarized in Table 1.<sup>[21–28]</sup> Inspection shows that some magnesium alloys exhibit excellent superplastic properties with reports of elongations exceeding 1000% in AZ91<sup>[24,27]</sup> and a Mg–8% Li alloy<sup>[25]</sup> but it is also apparent that there are no reports of superplastic flow in the AZ80 alloy after processing by HPT.

Among the commercially available Mg alloys, AZ80 alloys have a higher Al content which enhances their vulnerability toward stress corrosion cracking in alloys with significant quantities of  $\beta$ -phases.<sup>[29]</sup> In practice, the higher aluminum content in the AZ80 alloy offers greater strength than for the AZ31 alloy but generally with a much lower ductility. To make components of complex shapes, superplastic forming techniques are necessary for the manufacturing process after initial thermomechanical processing using procedures such as rolling, forging, ECAP, and HPT. Nevertheless, it is apparent there are no reports of superplasticity in the AZ80 magnesium alloy after processing by HPT even though this material has a demonstrated potential for use in numerous automotive applications.<sup>[28]</sup> The absence of any documented superplastic elongations in the AZ80 magnesium alloy after processing by HPT is surprising because there are reports of superplastic elongations of 541% at 573 K and 606% at

623 K<sup>[30,31]</sup> in this alloy after friction stir processing and 700% at 523 K in an AZ80%–1% Ca alloy after processing using high-ratio differential speed rolling.<sup>[32]</sup> There were also claims of superplasticity in a relatively coarse-grained extruded AZ80 with grain sizes larger than  $10 \mu\text{m}$  but the reported maximum elongations in these experiments were only 239% at 703 K<sup>[33]</sup> and 246% at 623 K<sup>[34]</sup> and these elongations fail to fulfill the fundamental requirement of an elongation of at least 400% for true superplastic flow. There are recent reviews of superplasticity in Mg alloys when using friction stir processing<sup>[35]</sup> and a range of SPD procedures<sup>[36]</sup> but these reviews confirm the absence of any data for superplastic flow in the AZ80 when processing by HPT.

Accordingly, the present investigation was initiated to evaluate the potential for achieving superplastic flow in the AZ80 alloy after processing by HPT. Several useful reports are now available describing the evolution of microstructure and the development of hardness in the AZ80 alloy when processing by HPT and other SPD techniques.<sup>[37–44]</sup> Thus, in the present research disks of a commercial AZ80 alloy were processed by HPT to produce an ultrafine grain size and then tensile specimens were cut from the disks and pulled to failure over a range of strain rates and testing temperatures to evaluate the potential for achieving superplastic elongations.

## 2. Material and Experimental Procedures

Experiments were conducted using a commercial AZ80 magnesium alloy supplied by Magnesium Electron Ltd. (Swinton, Manchester, UK). This alloy had a chemical composition (in wt%) of Al 8.7, Zn 0.51, Cu <0.001, Fe 0.005, Mn 0.18, Ni 0.0005, and Si 0.02 with the balance as Mg. The material was supplied in the form of extruded rods having diameters of 9.6 mm. Thin disks with thicknesses of  $\approx 1.5 \text{ mm}$  were sliced from the extruded rods and then ground with SiC abrasive papers from both sides to final thicknesses of  $\approx 0.85 \text{ mm}$ . This grinding effectively removed the strained surface layers from each disk.

The principle of processing by HPT is illustrated schematically in Figure 1.<sup>[45]</sup> The upper anvil remains stationary while the

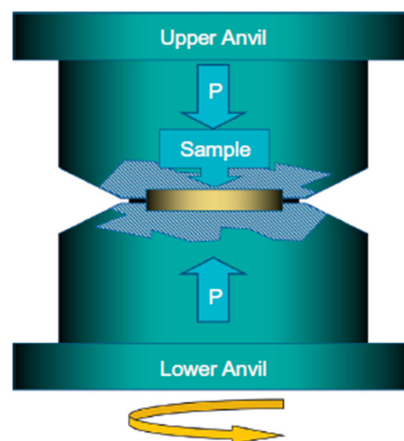


**Figure 1.** Schematic illustration of HPT processing illustrating the pressure applied on the sample (disk) and the torsional straining induced by the rotation of the lower anvil. Reproduced with permission.<sup>[45]</sup> Copyright 2008, Elsevier.

**Table 1.** Superplasticity in Mg alloys processed by HPT.

Material	Testing temperature [K]	Strain rate [ $\text{s}^{-1}$ ]	Maximum elongation	Reference
Mg–10% Gd	673	$1.0 \times 10^{-3}$	580%	[20]
Mg–9% Al	473	$5.0 \times 10^{-4}$	810%	[21]
AZ61	473	$3.3 \times 10^{-3}$	620%	[22]
ZK60	473	$1.0 \times 10^{-4}$	535%	[23]
AZ91	573	$1.0 \times 10^{-4}$	1308%	[24]
Mg–8% Li	473	$1.0 \times 10^{-3}$	1330%	[25]
Mg–8% Li	300	$1.0 \times 10^{-3}$	440%	[26]
AZ91	423	$1.0 \times 10^{-4}$	760%	[27]
AZ91	523	$1.0 \times 10^{-5}$	1150%	[27]



lower anvil rotates and both anvils have, on their inner surfaces, circular cavities of the same dimensions as the HPT disks. Each disk is then placed between the two anvils and subjected simultaneously to a high compressive pressure,  $P$ , and torsional straining. All disks were processed by HPT under quasiconstrained conditions where a limited amount of material flows out around the periphery of the disk in the gap between the upper and lower anvils during the straining operation.<sup>[46,47]</sup> This outflow helps to build the hydrostatic pressure on the disk and protect the anvils from damage.<sup>[48]</sup> The HPT processing was conducted at room temperature (RT, 296 K) through different numbers of turns,  $N$ , of  $\frac{1}{4}$ , 1, 3, 5, and 10 using an applied pressure of 6.0 GPa and a rotation speed of 1 rpm.

Following HPT, the processed disks were mechanically ground using SiC abrasive papers, polished to a final mirror-like surface, and the surfaces were then etched using an acetic-glycol solution (20 mL acetic acid + 19 mL water + 1 mL nitric acid + 60 mL ethylene). The microstructures were examined after HPT processing but before tensile testing using transmission electron microscopy (TEM) with a STEM Hitachi S-5500 microscope which provided an energy-dispersive X-ray spectroscopy (EDS) analysis of the matrix and the precipitates. Small foils of 3 mm diameter were punched from the HPT-processed disks and TEM foils were prepared by ion milling. The centers of the TEM foils were  $\approx 3$  mm from the centers of the HPT-processed disks and the foils were ground to a thickness of  $\approx 120$   $\mu\text{m}$ . Unprocessed disks were also inspected using scanning electron microscopy (SEM) with a JEOL JSM-6500F facility. The grain sizes of the HPT-processed samples were measured using the linear intercept method with image J with at least 30 grains measured from the TEM images and the mean grain size value was used for comparison purposes. The microhardness was measured using a hardness tester equipped with a Vickers indenter (FM300, Future-tech Corp.) under a load of 100 gf and with a dwell time of 10 s.

Miniature tensile specimens were carefully cut from the processed disks using electrodischarge machining (EDM) after reducing the disk thicknesses to  $\approx 0.65$  mm with SiC abrasive papers. **Figure 2** shows the positions and dimensions of the miniature tensile specimens cut from each HPT-processed disk. To avoid the higher heterogeneous microstructural area at the center of each disk,<sup>[48]</sup> two off-center samples were cut from each disk using the procedure described earlier<sup>[49]</sup> where the center of each tensile specimen was located 2 mm from the center of the disk. The gauge lengths and widths of these tensile specimens were 1.1 and 1.0 mm, respectively. In order to ensure accurate mechanical data for each specimen, and noting there are minor differences in thickness between the different specimens, the sectional measurements were carefully recorded before tensile testing. In addition, the reproducibility was checked by conducting each test 3 times for all testing conditions.

Tensile testing was performed at three different temperatures of 473, 523, and 573 K using a furnace surrounding the grips of a Zwick/Roell Z030 testing machine operating at a constant rate of cross-head displacement. Before starting each test, the samples were held at the testing temperature for 10 min to achieve thermal stability. All samples were pulled to failure in tension using strain rates of  $1.4 \times 10^{-4}$ ,  $1.4 \times 10^{-3}$ ,  $1.4 \times 10^{-2}$ , and  $1.4 \times 10^{-1} \text{ s}^{-1}$  for each testing temperature and for samples

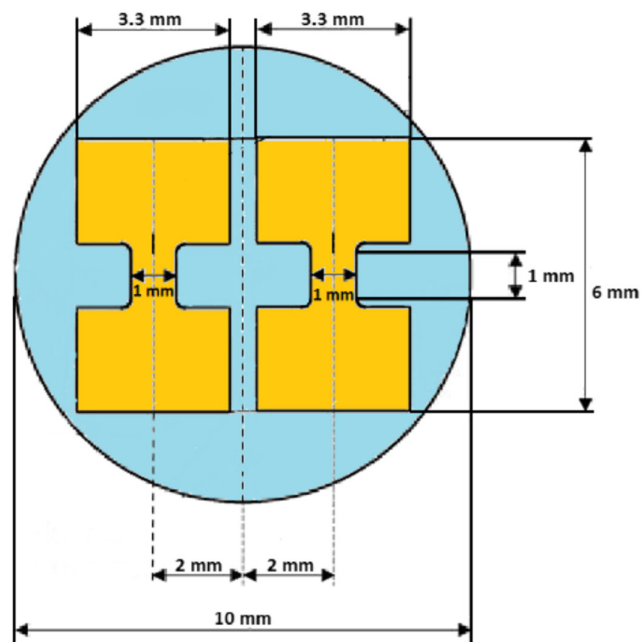


**Figure 2.** The position and dimensions of the miniature tensile specimens cut from the HPT-processed disk.

processed through  $\frac{1}{4}$ , 1, 3, 5, and 10 turns. The testing loads and displacements were recorded using testIXpert testing software in a computer-acquisition system. Following the tensile testing, the microstructures of the samples were observed using SEM at the gauge surfaces near the fracture tips without any further grinding or polishing. Optical microscopy (OM) images were also recorded to provide accurate calculations of the total elongations.

### 3. Experimental Results

**Figure 3** shows an SEM image of the microstructure of the AZ80 alloy in the as-received condition. Inspection confirmed an earlier report using OM of the presence of a homogeneous microstructure with an average grain size of  $\approx 25$   $\mu\text{m}$ . Measurements on the disk surface gave an average Vickers microhardness,

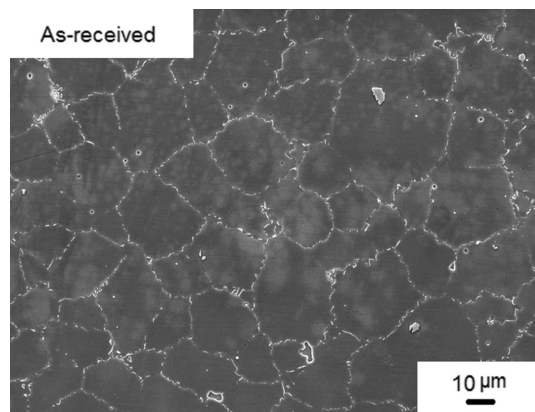


**Figure 3.** SEM image showing microstructure in the as-received condition of the AZ80 alloy.



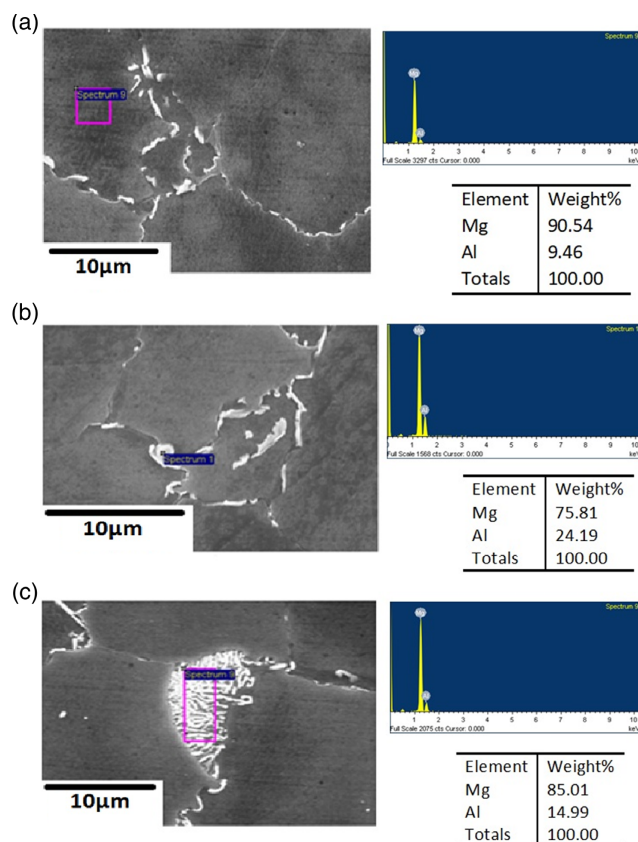


**Figure 4.** Chemical analysis of a) the matrix, b,c) precipitates ( $\text{Mg}_{17}\text{Al}_{12}$ ) of the alloy in the as-received condition and the EDS showing the weight percentage of the elements.

Hv, of  $\approx 63$ .<sup>[39]</sup> It is also apparent from inspection that the initial microstructure consists of two phases with an  $\alpha$ -phase as the matrix and a  $\beta$ -phase. The chemical compositions of the matrix Mg-rich phase and the secondary  $\beta$ -phase were analyzed using EDS, as shown in **Figure 4**. As the  $\beta$ -phase precipitates were rich in elemental aluminum, the precipitates were identified as  $\text{Mg}_{17}\text{Al}_{12}$  which is consistent with many earlier studies.<sup>[34,50,51]</sup> These precipitates were located primarily at the grain boundaries with average sizes of the order of several microns.

Processing the material by HPT gave a heterogeneous microstructure in the early stages of processing due to the variations in the imposed strain across the disks. **Figure 5** shows representative TEM images after processing through (a) 1, (b) 3, and (c) 5 turns with images of 1 and 3 turns revealing a mixture of fine and larger grains. The measured average grain sizes and the average values of Hv are summarized in **Table 2** and the measurements show that there is a reduction in grain size and an increase in hardness with increasing numbers of turns. Thus, the average grain size after one turn was  $\approx 370$  nm but this was reduced to  $\approx 200$  nm after 5 and 10 turns, as shown in **Figure 5c** and **6**. The development of a stable grain size after 5 and 10 turns is consistent with an earlier study on AZ31 processed by HPT at 296 K using an applied pressure of 6.0 GPa where there was a reasonably stable microstructural homogeneity after processing through 5 turns.<sup>[12]</sup> Inspection showed also that during the HPT

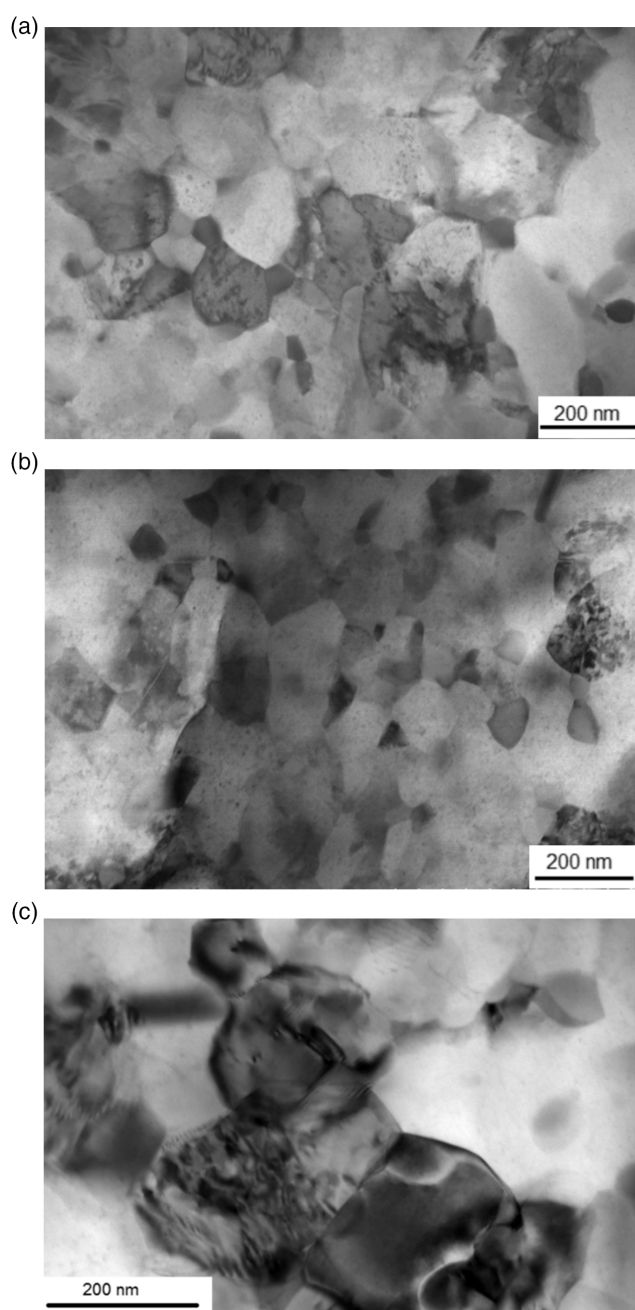


**Figure 5.** TEM images showing the microstructure of the AZ80 magnesium alloy processed by HPT at room temperature using an applied pressure of 6.0 GPa through a) 1, b) 3, and c) 5 turns.

processing the intermetallic  $\text{Mg}_{17}\text{Al}_{12}$   $\beta$ -phase became fragmented into nanosized particles located at the triple junction and these particles had average sizes of  $\approx 30$  nm after 10 turns as is evident in the TEM image in **Figure 7**. The line scanings of the chemical elements on the right in **Figure 7** confirm the analysis of the matrix and the precipitate phases after processing through 10 turns.

The main emphasis in this study was placed on tensile testing and the results are shown in **Figure 8** after testing at

**Table 2.** Average grain size and average microhardness values of the AZ80 alloy processed by HPT for different numbers of turns at 296 K using an applied pressure of 6.0 GPa.

Number of HPT turns	Average Vickers microhardness [Hv]	Average grain size [nm]
1	104	≈370
3	118	≈280
5	120	≈220
10	120	≈200

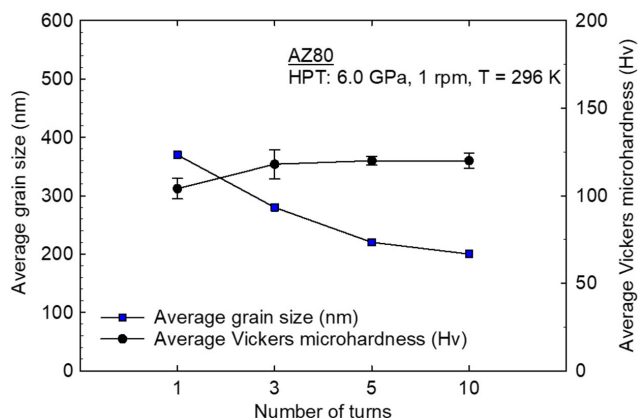


**Figure 6.** Average grain size and the average microhardness values of the alloy processed by HPT for different numbers of turns.

temperatures of 473, 523, and 573 K for strain rates from  $10^{-4}$  to  $10^{-1} \text{ s}^{-1}$  through (a) 1/4, (b) 1, (c) 3, (d) 5, and (e) 10 turns, respectively: the broken horizontal lines in these plots denote the limiting lower elongation of 400% which is required for superplastic flow and all experimental points above these lines show the occurrence of true superplasticity. In these plots, the

peak elongations were achieved in samples tested at the lowest strain rate of  $1.4 \times 10^{-4} \text{ s}^{-1}$  as shown in all plots. The maximum elongation was 645% which occurred in the sample tested at 573 K after only 1 turn of HPT, as shown in Figure 8b. It is important to note from these plots that superplasticity was achieved under all testing conditions even after processing by HPT through only 1/4 turn. There is also very clear evidence for low-temperature superplasticity at 473 K when processing through 1 and 3 turns but at this temperature superplastic flow was not achieved after processing through only 1/4 turn. Thus, the occurrence of superplastic flow in the AZ80 alloy depends critically on the testing temperature and the strain rate such that the maximum elongations to failure increase both with decreasing strain rate and with increasing testing temperature.

The appearance of representative samples is shown in Figure 9 and 10 for tests conducted over a range of experimental conditions. Figure 9 shows samples tested at 573 K at a strain rate of  $1.4 \times 10^{-4} \text{ s}^{-1}$  after processing by HPT through 1/4 to 10 turns and Figure 10 shows samples pulled to failure at 573 K after processing through 1 HPT turn and pulling to failure over a range of strain rates: in Figure 9 and 10 the upper samples were processed by HPT but not pulled in tension. A maximum elongation of 645% was achieved in the sample processed by HPT for 1 turn and tested at a strain rate of  $1.4 \times 10^{-4} \text{ s}^{-1}$ . Figure 9 and 10 illustrate that the AZ80 magnesium alloy does not follow the predicted trend of increasing superplasticity with increasing numbers of HPT processing turns and decreasing grain size as described earlier for an AZ91 magnesium alloy<sup>[24]</sup> but there are similarities to the earlier results reported for the ZK60 alloy after ECAP processing where the maximum superplasticity was achieved after the relatively small number of 2 passes through the ECAP die.<sup>[16]</sup> This latter result for ZK60 was attributed to the requirement for both grain refinement and structural stability in order to achieve high superplastic elongations. As there is extensive microstructural refinement in the AZ80 magnesium alloy from low numbers of turns in HPT, all specimens from the different numbers of HPT rotations exhibit

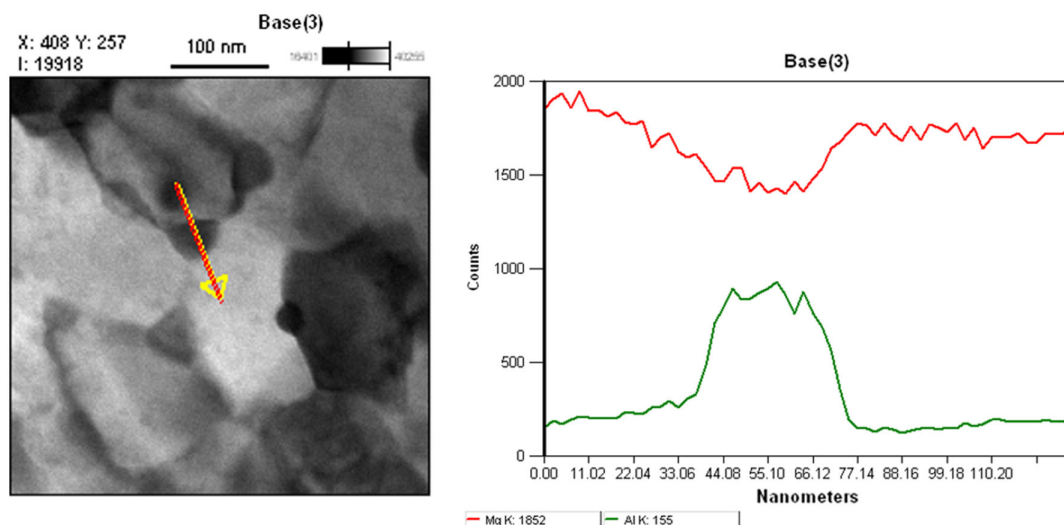


**Figure 7.** The precipitates at grain boundaries and triple junctions in the sample after 10 turns: TEM image (left) and the EDS line scanning (right) demonstrating the changes in chemical composition of the matrix and precipitates.

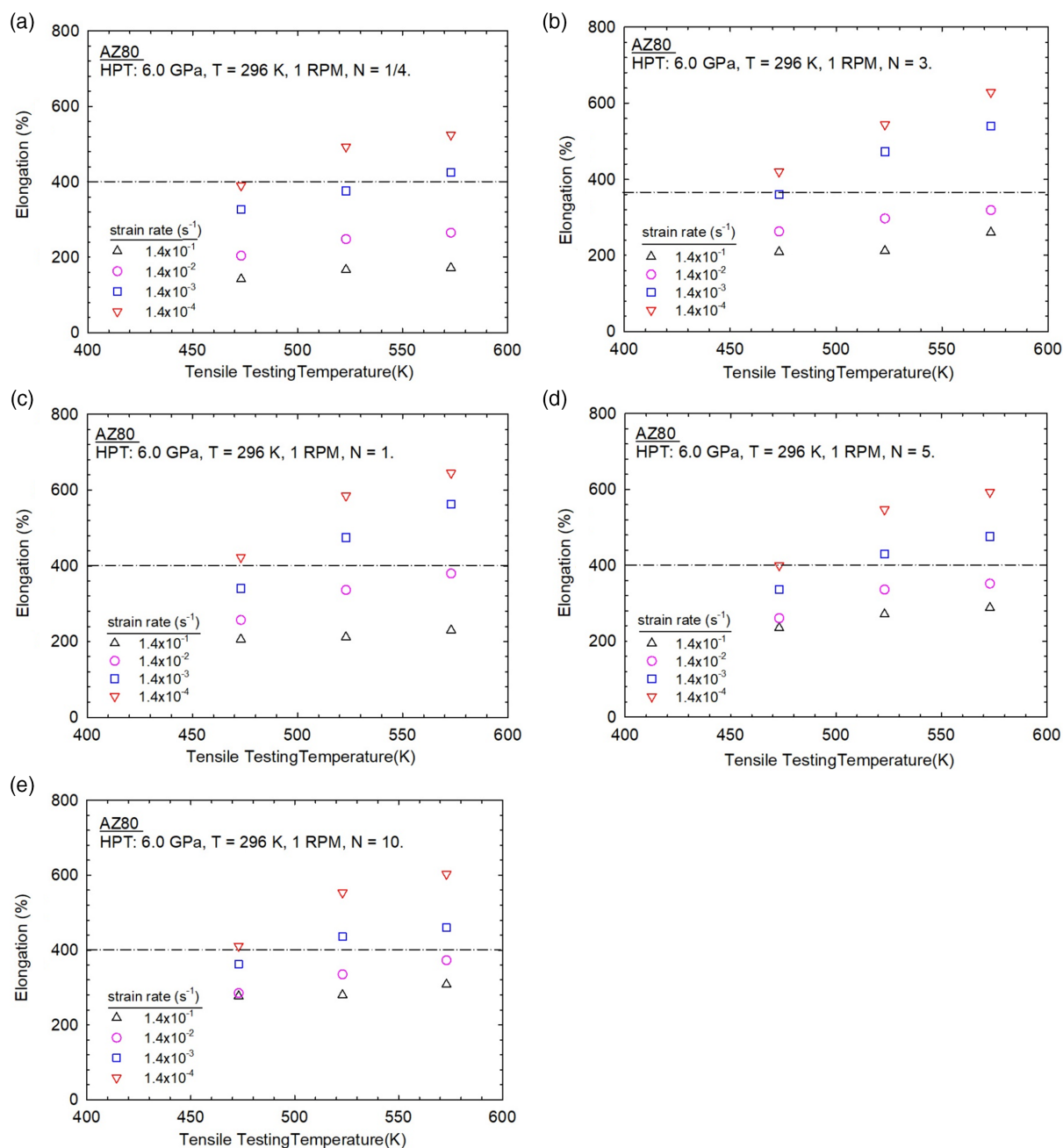


**Figure 8.** Elongation to failure of the AZ80 alloy processed by HPT for a) 1/4, b) 1, c) 3, d) 5, and e) 10 turns at room temperature using an applied pressure of 6.0 GPa and testing in tension for strain rates from  $10^{-4}$  to  $10^{-1} s^{-1}$  versus the tensile testing temperatures of 473, 523, and 573 K.

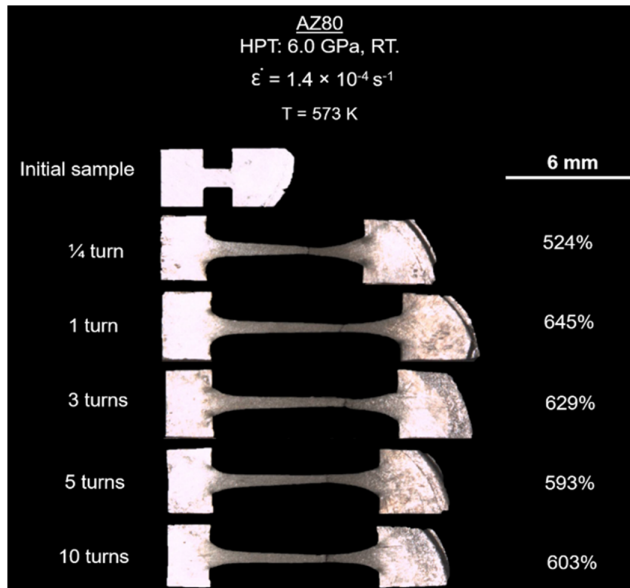
excellent elongations when tested to failure in tension with a strain rate of  $1.4 \times 10^{-4} s^{-1}$  and a testing temperature of 573 K, as illustrated in Figure 9.

Figure 10 demonstrates the effect of the testing strain rate on the final elongation when all samples are processed by HPT for 1 turn and pulled to failure in tension at 573 K using strain rates in the range of  $1.4 \times 10^{-4}$  to  $1.4 \times 10^{-1} s^{-1}$ . The samples tested at the two highest strain rates of  $1.4 \times 10^{-2}$  and  $1.4 \times 10^{-1} s^{-1}$  show good elongations of 380% and 230%, respectively, but these elongations are outside of the range for superplastic behavior. By contrast, the samples tested at the slower strain rates of

$1.4 \times 10^{-4}$  and  $1.4 \times 10^{-3} s^{-1}$  at a temperature of 573 K exhibit superplastic elongations of 645% and 563%, respectively. Both Figure 9 and 10 illustrate the occurrence of uniform deformation within the gauge lengths in superplastic flow without any visible necking at the fracture tips. This neck-free deformation is a fundamental requirement for superplastic behavior.<sup>[52]</sup>

The engineering stress-strain curves are shown in Figure 11 for samples processed by HPT for (a) 1 turn and (b) 10 turns and pulled in tension to failure at 573 K for a range of strain rates from  $1.4 \times 10^{-4}$  to  $1.4 \times 10^{-1} s^{-1}$ . At the lowest strain rate, the alloy exhibits a low strain hardening behavior with no peak





**Figure 9.** Samples processed by HPT at room temperature under an applied pressure of 6.0 GPa for different numbers of turns after pulling to failure in tension at a testing temperature of 573 K and a strain rate of  $1.4 \times 10^{-4} \text{ s}^{-1}$ : an untested sample is also shown.

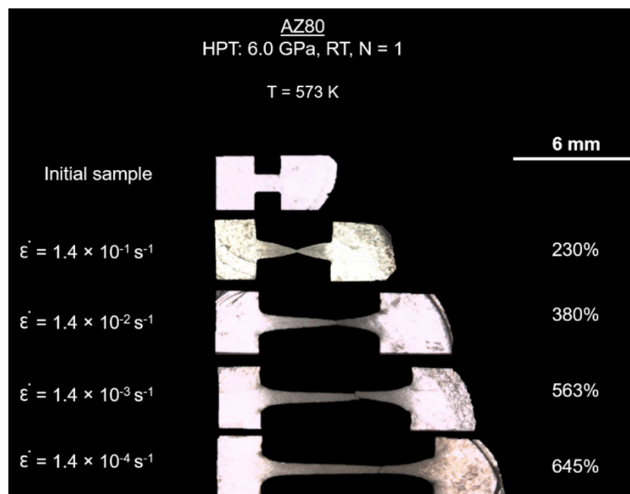


**Figure 10.** Samples processed by HPT at room temperature under an applied pressure of 6.0 GPa for  $N = 1$  turn after pulling to failure at a tensile testing temperature of 573 K using different strain rates from  $1.4 \times 10^{-4}$  to  $1.4 \times 10^{-1} \text{ s}^{-1}$ : an untested sample is also shown.

stress but the strain hardening increases with increasing strain rate and there is a consequent decrease in the total elongation.

The SEM images in **Figure 12a–d** show the grains within the gauge lengths after tensile testing to failure at 573 K without any additional preparation of the samples where the left column is for  $N = 1$  turn and the right column is for  $N = 10$  turns. Thus, the grains are equiaxed and distributed relatively homogeneously on the surfaces of all these elongated specimens with clear evidence for cavities and interspaces between the grains as denoted by the

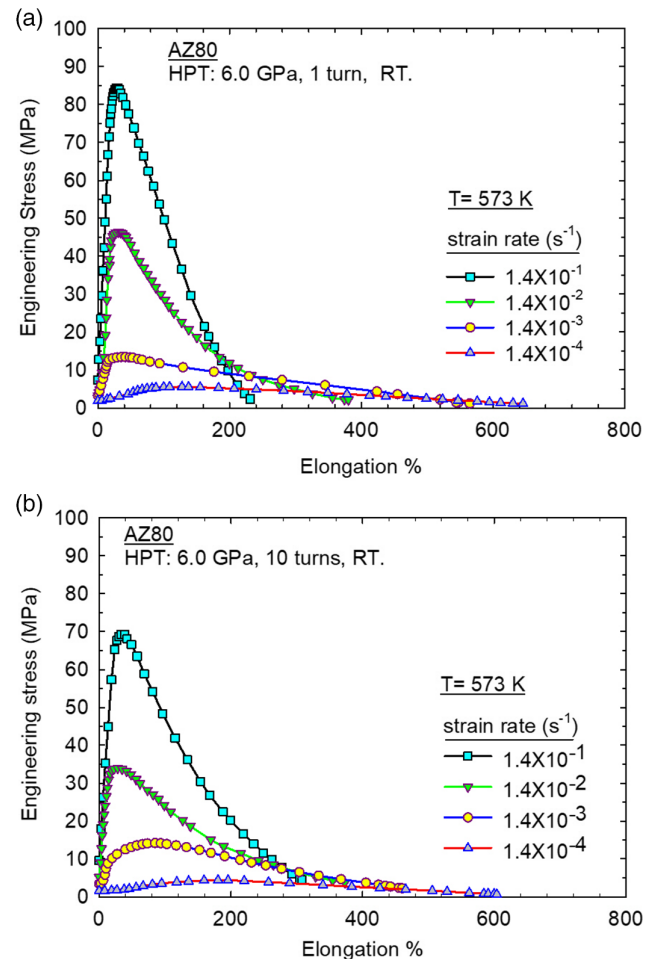


**Figure 11.** Engineering stress–strain curves for the AZ80 alloy processed for a)  $N = 1$  and b)  $N = 10$  turns of HPT at room temperature using an applied pressure of 6.0 GPa and tested in tension at different strain rates at a temperature of 573 K.

yellow arrows. Using the faster strain rate of  $1.4 \times 10^{-2} \text{ s}^{-1}$ , the grain size after 10 turns in (b) is clearly smaller than the grain size after 1 turn in (a), whereas when testing at the slower rate of  $1.4 \times 10^{-4} \text{ s}^{-1}$  the grains are smaller after 1 turn in (c) than after 10 turns in (d). There is also evidence for the existence of filaments between the grains as shown in **Figure 12a,c,d** and denoted by red arrows. These filaments suggest the presence of high viscosity areas along the grain boundaries<sup>[37]</sup> where this high viscosity phase tolerates a large number of cavities before fracture of the sample. Thus, these filaments act to connect the grains by filling in the cavities and spaces between them.

The strain rate sensitivity,  $m$ , was estimated from the stress–strain data in **Figure 11** and the results are presented in **Figure 13** for (a) 1 turn and (b) 10 turns where it is apparent that the value of  $m$  tends to increase with decreasing strain rate. The value of  $m$  was  $\approx 0.52$  under conditions of maximum superplasticity after processing by HPT for 1 turn and pulling in tension to failure. Inspection shows that superplasticity can be achieved over a wider strain rate range after processing by HPT for 1 turn

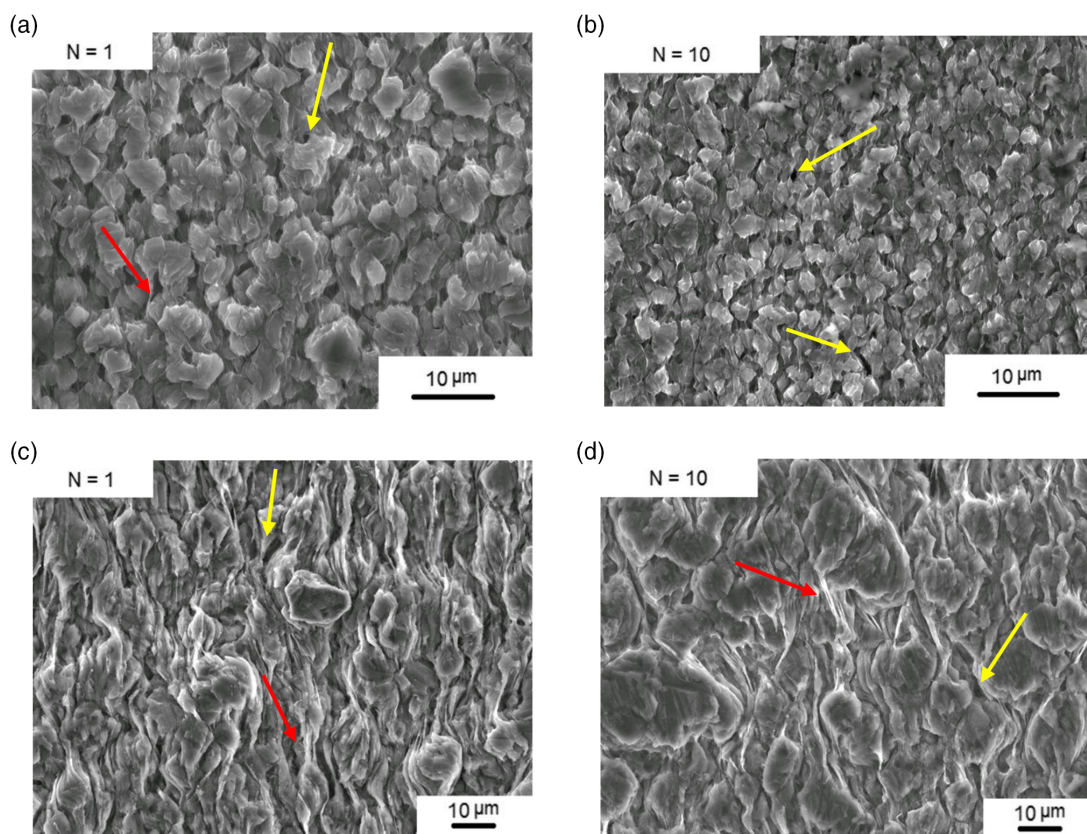


**Figure 12.** SEM images of the grains within the gauge lengths of the samples after tensile testing to failure at 573 K where a)  $N = 1$  and b)  $N = 10$  with testing strain rate of  $1.4 \times 10^{-2} \text{ s}^{-1}$ , c)  $N = 1$ , and d)  $N = 10$  with testing strain rate of  $1.4 \times 10^{-4} \text{ s}^{-1}$  showing cavities and interspaces (marked by yellow arrows) and filaments (marked by red arrows).

whereas processing at 10 turns produces an  $m$  value of  $\approx 0.5$  only at the slowest strain rates of  $1.4 \times 10^{-4}$  and  $1.4 \times 10^{-3} \text{ s}^{-1}$ . This is consistent with the measured elongations shown in Figure 8e.

## 4. Discussion

### 4.1. Microstructural Characteristics after HPT Processing

The results of this investigation demonstrate that the HPT processing of the AZ80 magnesium alloy at a temperature of 296 K was successful because it produced an ultrafine-grained microstructure of reasonable homogeneity with an average grain size of the order of  $\approx 200 \text{ nm}$ . A similar grain refinement was reported earlier for the magnesium AZ80,<sup>[37,39]</sup> AZ31,<sup>[53]</sup> and AZ91<sup>[24]</sup> alloys after processing by HPT. In the early stages of HPT processing, the microstructure contained both fine and coarse grains as shown by the TEM image in Figure 5a after 1 turn, but the microstructure developed gradually into a reasonably uniform ultrafine grain structure after 10 turns of HPT processing, as shown in Figure 7.

It is well-established that the morphology and distribution of any second phase may play a role in material strengthening. In the present experiments, an intermetallic  $\beta$  ( $\text{Mg}_{17}\text{Al}_{12}$ ) phase was precipitated at the grain boundaries with an initial average size of several microns which, based on results for the AZ31

alloy,<sup>[54]</sup> is too large to effectively impede the movement of dislocations. Nevertheless, during the HPT processing these precipitates are broken into fine particles and become highly deformed with an average size of several nanometers. These fine particles are located at the triple junctions between the ultrafine grains as shown in Figure 7 and this enhances the strength of the alloy by providing a general resistance to dislocation slip<sup>[55]</sup> when pulling in tension at elevated temperatures. These fine particles also inhibit grain growth and this improves the magnitude of the superplastic flow.<sup>[56]</sup>

### 4.2. The Characteristics of Superplasticity in the AZ80 Alloy

A maximum elongation of 645% was achieved in the AZ80 alloy when testing at 573 K where this represents the first demonstration of true superplastic flow in an AZ80 alloy when testing after processing by HPT. The temperature of 573 K corresponds to a homologous temperature of  $\approx 0.65 T_m$  where  $T_m$  is the absolute melting temperature which is taken as 883 K based on the Mg–Al binary phase diagram. In addition, there was a maximum elongation of 423% at the lower testing temperature of 473 K, equivalent to  $\approx 0.53 T_m$ , which demonstrates the occurrence of low-temperature superplasticity. Other magnesium alloys such as the Mg–9% Al alloy processed by HPT and pulled to failure at 473 K ( $\approx 0.62 T_m$ ) with an initial strain rate of  $5.0 \times 10^{-4} \text{ s}^{-1}$

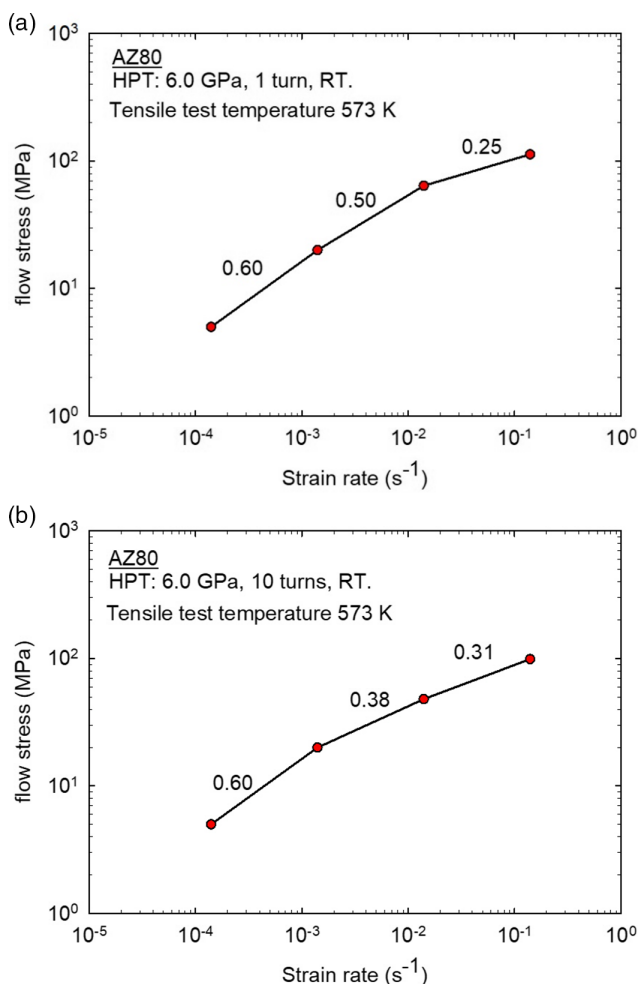


**Figure 13.** Strain rate sensitivity of samples processed by HPT at room temperature for a) 1 and b) 10 turns and tested to failure in tension using a range of strain rates at 573 K.

gave an elongation of 810%<sup>[19]</sup> and the HPT-processed AZ91 alloy gave elongations of 1308% at 573 K ( $\approx 0.74 T_m$ ) with an initial strain rate of  $1.0 \times 10^{-4} \text{ s}^{-1}$ <sup>[22]</sup> and 1070% and 1150% at 523 K ( $\approx 0.68 T_m$ ) with initial strain rates of  $1.0 \times 10^{-4}$  and  $1.0 \times 10^{-5} \text{ s}^{-1}$ .<sup>[27]</sup>

It is important to note that the AZ91 and AZ80 alloys are both alloys in the Mg–Al–Zn system but the increased Al content in the AZ91 alloy suggests that more intermetallic  $\beta$ -phase ( $\text{Mg}_{17}\text{Al}_{12}$ ) will precipitate at the grain boundaries in this alloy than in the AZ80 alloy.<sup>[57]</sup> Therefore, the higher superplastic elongations in the HPT-processed AZ91 alloy compared with the HPT-processed AZ80 alloy are due to the presence of a higher fraction of nanosized  $\beta$ -phase ( $\text{Mg}_{17}\text{Al}_{12}$ ) particles over the grain boundary areas in the AZ91 alloy because this effectively pins the grain boundaries, impedes grain growth, and thereby improves the superplastic capability.

The optimum superplastic behavior was obtained in this research after only 1 turn at the slow strain rate of  $1.4 \times 10^{-4} \text{ s}^{-1}$  at 573 K. This is consistent with earlier results on a ZK60 magnesium alloy processed by ECAP and tested at 473 K at a strain

rate of  $10^{-4} \text{ s}^{-1}$  where the maximum elongation of 3050% was obtained after two passes of ECAP and an elongation of only 930% was reported after six passes of ECAP.<sup>[16]</sup> Earlier investigations showed also that the presence of a bimodal microstructure may facilitate dislocation movement as an accommodating mechanism in superplasticity due to the ease of generating slip in the coarser grains<sup>[58]</sup> and there are reports of the development of a transition microstructure consisting of fine and coarse grains in the early stages of HPT processing.<sup>[12]</sup> The presence of a bimodal microstructure is evident in the present investigation after 1 turn of HPT as shown in Figure 5a. Thus, all of these factors, including a bimodal microstructure, nanosized  $\text{Mg}_{17}\text{Al}_{12}$  particles pinning the grain boundaries and an appropriate temperature to activate additional nonbasal  $\langle c + a \rangle$  slip systems, will contribute to achieving a maximum elongation in the AZ80 alloy when the sample is processed through a small number of turns of HPT.

It is important to note also that the maximum elongation of 645% was achieved using a small specimen with gauge length of 1.1 mm, width of 1.0 mm, and, due to the limitation imposed by the size of the HPT disk, an initial thickness of  $< 0.65 \text{ mm}$ . It is reasonable to anticipate that larger specimens will exhibit longer elongation due to the greater volume of material which is then available to participate in the deformation process whereas in the present research the overall elongations are limited by the exceptionally small thicknesses of the tensile samples.

The maximum elongations obtained at the testing temperature of 473 K were lower than at 573 K and these increased elongations at the higher temperatures are consistent with the activation of nonbasal slip systems.<sup>[33]</sup> Thus, increasing the temperature above  $\approx 500 \text{ K}$  will activate additional nonbasal  $\langle c + a \rangle$  slip systems<sup>[4]</sup> and give enhanced formability and ductility when testing at 573 K.

The microstructures of the samples were investigated within the gauge lengths after tensile testing at 573 K as shown in Figure 12a–d for samples processed by HPT for 1 and 10 turns at strain rates of (a,b)  $1.4 \times 10^{-2} \text{ s}^{-1}$  and (c,d)  $1.4 \times 10^{-4} \text{ s}^{-1}$ , respectively. Inspection shows the grains in the superplastic regime are equiaxed and their sizes are  $< 10 \mu\text{m}$  which is the conventional requirement for superplastic flow.<sup>[59]</sup> Thus, there was grain stability and the ultrafine grain size was retained when testing at an elevated temperature.

#### 4.3. The Deformation Mechanism for Superplastic Flow in the AZ80 Alloy

Superplasticity denotes the exceptionally high elongations that may be achieved in some materials when testing in tension. This process requires very small grains, typically  $< 10 \mu\text{m}$ ,<sup>[59]</sup> and an important feature of superplastic flow is that the grains retain their equiaxed configuration even at very high strains. Inspection suggests that flow occurs by the movement of grains over each other in the process of grain boundary sliding (GBS)<sup>[60]</sup> but this requires an accommodation process such as the intragranular movement of dislocations. Several experimental results are now available confirming the movement of dislocations as an accommodating process in superplasticity<sup>[61–64]</sup> and a



mechanism was developed based on GBS accommodated by dislocation slip.<sup>[65]</sup> This mechanism predicts a strain rate sensitivity of  $m = 0.5$ , an inverse dependence on grain size raised to the power of 2, and an activation energy for superplastic flow equal to the value for grain boundary diffusion.

In this research on the AZ80 alloy, superplastic flow occurs under conditions where the value of  $m$  is close to 0.5 as shown by the results in Figure 13a but it is not possible to deduce the dependence on grain size because the initial grain size was not varied in these experiments. In order to estimate the value of the activation energy for superplasticity,  $Q$ , it is first necessary to express the steady-state strain rate,  $\dot{\epsilon}$ , in the form of the conventional relationship given by<sup>[65]</sup>

$$\dot{\epsilon} = \frac{ADGb}{kT} \left( \frac{b}{d} \right)^2 \left( \frac{\sigma}{G} \right)^2 \quad (1)$$

where  $D$  is the diffusion coefficient equal to grain boundary diffusion in superplastic flow ( $=D_o \exp(-Q/RT)$ , where  $D_o$  is a frequency factor,  $Q$  is the appropriate activation energy for diffusion, and  $R$  is the gas constant),  $G$  is the shear modulus,  $b$  is the Burgers vector,  $k$  is the Boltzmann's constant,  $d$  is the grain size,  $A$  is a constant having a value of  $\approx 10$  for superplasticity, and the stress exponent,  $n$ , is equal to 2 which gives a strain rate sensitivity of  $m = 1/n = 0.5$ . It follows from Equation (1) that it is possible to determine the activation energy by taking  $n = 2$  and plotting the flow stress against the reciprocal of temperature for samples tested at constant strain rates.

The result is shown in Figure 14 where data are plotted for the two lowest strain rates of  $1.4 \times 10^{-4}$  and  $1.4 \times 10^{-3} \text{ s}^{-1}$  for samples tested at temperatures of 473, 523, and 573 K after processing by HPT through  $N = 1$  turn. From these results, the activation energy for superplasticity is estimated as  $Q = 73 \text{ kJ mol}^{-1}$ . This value is significantly lower than the self-diffusion activation energy for pure magnesium ( $135 \text{ kJ mol}^{-1}$ ) and it is also lower than the value generally taken for grain boundary diffusion in pure magnesium ( $92 \text{ kJ mol}^{-1}$ ).<sup>[66]</sup> However, it is similar to the values of 83.2 and  $69.9 \text{ kJ mol}^{-1}$  reported for the tensile creep

of Mg–4Al alloys<sup>[67]</sup> where these latter values were interpreted in terms of grain boundary diffusion.<sup>[68]</sup> Therefore, it is concluded that GBS is the rate-controlling deformation mechanism in the superplastic AZ80 alloy.

Finally, it is noted there is experimental evidence in Figure 12 for the development of cavities and interspaces between the grain and the formation of filaments disconnecting grains during superplastic flow. These observations are similar to other reports for superplastic materials and they are also consistent with GBS as the flow process.<sup>[69,70]</sup>

## 5. Conclusions

1) Experiments were conducted to evaluate the potential for achieving superplastic elongations in the AZ80 magnesium alloy after processing by HPT. Tensile tests were conducted on the HPT-processed samples using a range of strain rates from  $1.4 \times 10^{-4}$  to  $1.4 \times 10^{-1} \text{ s}^{-1}$  and temperatures from 473 to 573 K. 2) Excellent superplastic properties were received in the alloy with a maximum elongation of 645% when testing with a strain rate of  $1.4 \times 10^{-4} \text{ s}^{-1}$  after processing through only 1 turn of HPT. A good superplastic elongation of 423% was also achieved at the lower testing temperature of 473 K after 1 turn of HPT when pulling at the same low strain rate. 3) Microstructural observations showed the grains were equiaxed after pulling to the highest superplastic elongations and superplasticity occurred with a strain rate sensitivity of  $\approx 0.5$ . The activation energy for superplastic flow was measured as  $\approx 73 \text{ kJ mol}^{-1}$  which is consistent with grain boundary sliding as the deformation mechanism.

## Acknowledgements

This work was supported by the European Research Council under ERC Grant Agreement No. 267464-SPDMETALS and by the Public Authority for Applied Education and Training in Kuwait.

## Conflict of Interest

The authors declare no conflict of interest.

## Data Availability Statement

The data that support the findings of this study are available from the corresponding author upon reasonable request.

## Keywords

high-pressure torsion, magnesium AZ80 alloys, severe plastic deformation, superplasticity, ultrafine grains

Received: April 28, 2022

Revised: May 29, 2022

Published online: July 3, 2022

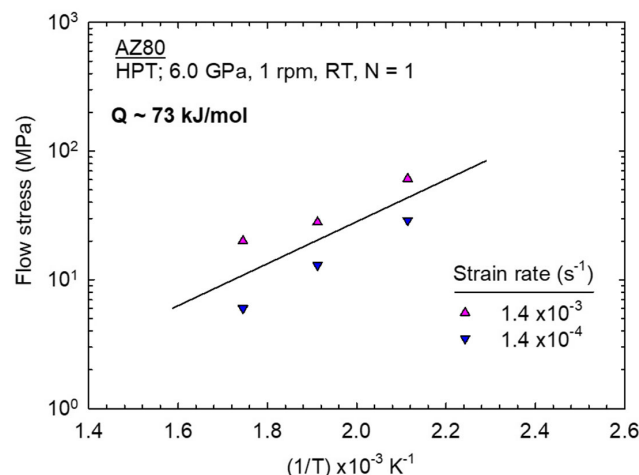


**Figure 14.** Variation of flow stress with the reciprocal of temperature for samples processed by HPT for 1 turn and tested in tension at strain rates of  $1.4 \times 10^{-4}$  and  $1.4 \times 10^{-3} \text{ s}^{-1}$ .

[1] B. Mordike, T. Ebert, *Mater. Sci. Eng. A* **2001**, 302, 37.

[2] T. M. Pollock, *Science* **2010**, 328, 986.

- [3] M. H. Yoo, *Metall. Trans. A* **1981**, 12, 409.
- [4] T. Al-Samman, G. Gottstein, *Mater. Sci. Eng. A* **2008**, 490, 411.
- [5] R. Z. Valiev, Y. Estrin, Z. Horita, T. G. Langdon, M. J. Zehetbauer, Y. T. Zhu, *JOM* **2006**, 58, 33.
- [6] R. Z. Valiev, Y. Estrin, Z. Horita, T. G. Langdon, M. J. Zehetbauer, Y. T. Zhu, *JOM* **2016**, 68, 1216.
- [7] R. Z. Valiev, Y. Estrin, Z. Horita, T. G. Langdon, M. J. Zehetbauer, Y. T. Zhu, *Mater. Res. Lett.* **2016**, 4, 1.
- [8] R. Z. Valiev, T. G. Langdon, *Prog. Mater. Sci.* **2006**, 51, 881.
- [9] A. P. Zhilyaev, T. G. Langdon, *Prog. Mater. Sci.* **2008**, 53, 893.
- [10] R. B. Figueiredo, P. R. Cetlin, T. G. Langdon, *Acta Mater.* **2007**, 55, 4769.
- [11] P. R. Cetlin, M. T. P. Aguilar, R. B. Figueiredo, T. G. Langdon, *J. Mater. Sci.* **2010**, 45, 4561.
- [12] Y. Huang, R. B. Figueiredo, T. Baudin, F. Brisset, T. G. Langdon, *Adv. Eng. Mater.* **2012**, 14, 1018.
- [13] R. B. Figueiredo, T. G. Langdon, *Adv. Eng. Mater.* **2019**, 21, 1801039.
- [14] T. G. Langdon, *J. Mater. Sci.* **2009**, 44, 5998.
- [15] A. J. Barnes, *J. Mater. Eng. Perform.* **2007**, 16, 440.
- [16] R. B. Figueiredo, T. G. Langdon, *Adv. Eng. Mater.* **2008**, 10, 37.
- [17] R. Z. Valiev, M. Y. Murashkin, A. Kilmametov, B. Straumal, N. Q. Chinh, T. G. Langdon, *J. Mater. Sci.* **2010**, 45, 4718.
- [18] M. Kawasaki, T. G. Langdon, *Mater. Sci. Eng. A* **2011**, 528, 6140.
- [19] M. Kawasaki, T. G. Langdon, *J. Mater. Sci.* **2014**, 49, 6487.
- [20] O. B. Kulyasova, R. K. Islamgaliev, A. R. Kil'mametov, R. Z. Valiev, *Phys. Metals Metallog.* **2006**, 101, 585.
- [21] M. Kai, Z. Horita, T. G. Langdon, *Mater. Sci. Eng. A* **2008**, 488, 117.
- [22] Y. Harai, M. Kai, K. Kaneko, Z. Horita, T. G. Langdon, *Mater. Trans.* **2008**, 49, 76.
- [23] S. A. Torbati-Sarraf, T. G. Langdon, *J. Alloys Compds.* **2014**, 613, 357.
- [24] A. S. J. Al-Zubaydi, A. P. Zhilyaev, S. C. Wang, P. A. S. Reed, *Mater. Sci. Eng. A* **2015**, 637, 1.
- [25] H. Matsunoshita, K. Edalati, M. Furui, Z. Horita, *Mater. Sci. Eng. A* **2015**, 640, 443.
- [26] K. Gusieva, C. H. J. Davies, J. R. Scully, N. Birbilis, *Int. Mater. Rev.* **2015**, 60, 169.
- [27] K. Edalati, T. Masuda, M. Arita, M. Furui, X. Sauvage, Z. Horita, R. Z. Valiev, *Sci. Rpts.* **2017**, 7, 2662.
- [28] R. B. Figueiredo, T. G. Langdon, *Metals* **2020**, 10, 681.
- [29] V. Kevorkian, *Mater. Sci. Tech.* **2003**, 19, 1386.
- [30] W. Wang, P. Han, P. Peng, H. Guo, L. Huang, K. Qiao, M. Hai, Q. Yang, H. Wang, K. Wang, L. Wang, *J. Mater. Res. Technol.* **2020**, 9, 5252.
- [31] Y. Takayama, I. Takeda, T. Shibayanagi, H. Kato, K. Funami, *Key Eng. Mater.* **2010**, 433, 241.
- [32] W. J. Kim, Y. G. Lee, *Mater. Lett.* **2010**, 64, 1759.
- [33] Z. Wang, Z. Wang, J. Zhu, *Adv. Mater. Lett.* **2011**, 2, 113.
- [34] L. Ren, J. Wu, G. Quan, *Mater. Sci. Eng. A* **2014**, 612, 278.
- [35] D. Harwani, V. Badheka, V. Patel, W. Li, J. Andersson, *J. Mater. Res. Technol.* **2021**, 12, 2055.
- [36] F. Nazeer, J. Long, Z. Yang, C. Li, *J. Magn. Alloys* **2022**, 10, 97.
- [37] D. Arpacay, S. Yi, M. Janeček, A. Bakaloglu, L. Wagner, *Mater. Sci. Forum* **2008**, 584–586, 300.
- [38] Q. Zhu, L. Li, Z. Zhang, Z. Zhao, Y. Zuo, J. Cui, *Mater. Trans.* **2014**, 55, 270.
- [39] S. A. Alsubaie, P. Bazarnik, M. Lewandowska, Y. Huang, T. G. Langdon, *J. Mater. Res. Tech.* **2016**, 5, 152.
- [40] S. Sepahi-Borouieni, A. Sepahi-Borouieni, *J. Manuf. Proc.* **2016**, 24, 71.
- [41] S. A. Alsubaie, Y. Huang, T. G. Langdon, *J. Mater. Res. Tech.* **2017**, 6, 378.
- [42] S. A. Alsubaie, Y. Huang, T. G. Langdon, *Mater. Sci. Forum* **2017**, 879, 139.
- [43] J. Zhang, H. Xie, Y. Ma, S. Tao, K. Zhao, W. Wu, *Mater. Sci.* **2019**, 25, 141.
- [44] N. X. Zhang, M. Kawasaki, H. Ding, T. G. Langdon, *Mater. Sci. Eng. A* **2021**, 606, 140832.
- [45] C. Xu, Z. Horita, T. G. Langdon, *Acta Mater.* **2008**, 56, 5168.
- [46] R. B. Figueiredo, P. R. Cetlin, T. G. Langdon, *Mater. Sci. Eng. A* **2011**, 528, 8198.
- [47] R. B. Figueiredo, P. H. R. Pereira, M. T. P. Aguilar, P. R. Cetlin, T. G. Langdon, *Acta Mater.* **2012**, 60, 3190.
- [48] A. Hohenwarter, A. Bachmaier, B. Gludovatz, S. Scheriau, R. Pippan, *Int. J. Mater. Res.* **2009**, 100, 1653.
- [49] A. Loucif, R. B. Figueiredo, M. Kawasaki, T. Baudin, F. Brisset, R. Chemam, T. G. Langdon, *J. Mater. Sci.* **2012**, 47, 7815.
- [50] B. Q. Shi, R. S. Chen, W. Ke, *Mater. Sci. Eng. A* **2012**, 546, 323.
- [51] L. Tang, Y. Zhao, R. K. Islamgaliev, C. Y. A. Tsao, R. Z. Valiev, E. J. Lavernia, Y. T. Zhu, *Mater. Sci. Eng. A* **2016**, 670, 280.
- [52] T. G. Langdon, *Met. Sci.* **1982**, 16, 175.
- [53] J. Stráská, M. Janeček, J. Gubicza, T. Krajňák, E. Y. Yoon, H. S. Kim, *Mater. Sci. Eng. A* **2015**, 625, 98.
- [54] P. Yang, L. N. Wang, Q. G. Xie, J. Z. Li, H. Ding, L. L. Lu, *Int. J. Miner. Metall. Mater.* **2011**, 18, 338.
- [55] M.-S. Tsai, P.-L. Sun, P.-W. Kao, C.-P. Chang, *Mater. Trans.* **2009**, 50, 771.
- [56] S. W. Xu, S. Kamado, N. Matsumoto, T. Honma, Y. Kojima, *Mater. Sci. Eng. A* **2009**, 527, 52.
- [57] N. P. Papenberg, S. Gneiger, I. Weißensteiner, P. J. Uggowitzer, S. Pogatscher, *Materials* **2020**, 13, 985.
- [58] R. Lapovok, Y. Estrin, M. V. Popov, T. G. Langdon, *Adv. Eng. Mater.* **2008**, 10, 429.
- [59] T. G. Langdon, *Metall. Trans. A* **1982**, 13A, 689.
- [60] T. G. Langdon, *Mater. Sci. Eng. A* **1994**, 174, 225.
- [61] L. K. L. Falk, P. R. Howell, G. L. Dunlop, T. G. Langdon, *Acta Metall.* **1986**, 34, 1203.
- [62] R. Z. Valiev, T. G. Langdon, *Acta Metall. Mater.* **1993**, 41, 949.
- [63] Y. Xun, F. A. Mohamed, *Phil. Mag.* **2003**, 83, 2247.
- [64] Y. Xun, F. A. Mohamed, *Acta Mater.* **2004**, 52, 4401.
- [65] T. G. Langdon, *Acta Metall. Mater.* **1994**, 42, 2437.
- [66] H. J. Forst, M. F. Ashby, *Deformation-Mechanism Maps: The Plasticity and Creep of Metals and Ceramics*, Pergamon Press, Oxford, UK **1982**.
- [67] J. Bai, Y. S. Sun, S. Xun, F. Xue, T. B. Zhu, *Mater. Sci. Eng. A* **2006**, 419, 181.
- [68] M. O. Pekgulyeryuz, A. A. Kaya, *Adv. Eng. Mater.* **2003**, 5, 866.
- [69] L. Clarisse, A. Bataille, Y. Pennec, J. Crampon, R. Duclos, *Ceram. Int.* **1999**, 25, 389.
- [70] T. Mohri, M. Mabuchi, M. Nakamura, T. Asahina, H. Iwasaki, T. Aizawa, K. Higashi, *Mater. Sci. Eng. A* **2000**, 290, 139.